Generation of 20 kA electron beam from a laser wakefield accelerator

Cite as: Phys. Plasmas **24**, 023108 (2017); https://doi.org/10.1063/1.4975613
Submitted: 27 October 2016 • Accepted: 20 January 2017 • Published Online: 09 February 2017

Y. F. Li, D. Z. Li, K. Huang, et al.

Generation of 20 kA electron beam from a laser wakefield accelerator

Y. F. Li,[1] D. Z. Li,[2,a)] K. Huang,[1,3] M. Z. Tao,[1] M. H. Li,[1] J. R. Zhao,[1] Y. Ma,[1] X. Guo,[1] J. G. Wang,[1] M. Chen,[4,5] N. Hafz,[4,5] J. Zhang,[4,5] and L. M. Chen[1,4,5,6,a)]
[1]*Beijing National Laboratory of Condensed Matter Physics, Institute of Physics, CAS, Beijing 100190, China*
[2]*Institute of High Energy Physics, CAS, Beijing 100049, China*
[3]*Kansai Photon Science Institute (KPSI), National Institutes for Quantum and Radiological Science and Technology (QST), 8-1-7 Umemidai, Kizugawa, Kyoto 619-0215, Japan*
[4]*Key Laboratory for Laser Plasmas (MOE) and Department of Physics and Astronomy, Shanghai Jiao Tong University, Shanghai 200240, China*
[5]*Collaborative Innovation Center of IFSA, Shanghai Jiao Tong University, Shanghai 200240, China*
[6]*School of Physical Sciences, University of Chinese Academy of Sciences, Beijing 100049, China*

(Received 27 October 2016; accepted 20 January 2017; published online 9 February 2017)

We present the experimentally generated electron bunch from laser-wakefield acceleration (LWFA) with a charge of 620 pC and a maximum energy up to 0.6 GeV by irradiating 80 TW laser pulses at a 3 mm Helium gas jet. The charge of injected electrons is much larger than the normal scaling laws of LWFA in bubble regime. We also got a quasi-monoenergetic electron beam with energy peaked at 249 MeV and a charge of 68 pC with the similar laser conditions but lower plasma density. As confirmed by 2D particle-in-cell simulations, the boosted bunch charge is due to the continuous injection caused by the self-steepening and self-compression of a laser pulse. During the nonlinear evolution of the laser pulse, the bubble structure broadens and stretches, leading to a longer dephasing length and larger beam charge. *Published by AIP Publishing.*
[http://dx.doi.org/10.1063/1.4975613]

I. INTRODUCTION

Since Tajima and Dawson[1] proposed the concept of laser-wakefield acceleration (LWFA) in 1979, the LWFA has been regarded as a promising scheme to realize a table-top accelerator for generating energetic electron (∼GeV) beams with the quasi-monoenergetic spectrum due to its extremely large accelerating gradient. A significant progress was achieved in generating quasi-monoenergetic electron beams experimentally.[2–4] After that, a tremendous amount of experiments were performed, and great progresses have been achieved in increasing the electron energy up to multi-GeV and improving the quality of electron beams.[5–11] Most of those experiments were performed at the so-called blowout or "bubble" regime, where the electrons are expelled from the focal region of the laser by the ponderomotive force of the laser pulse, forming an electron sheath surrounding the ion cavity. The electric field within the bubble varies approximately linearly in all three spatial dimensions of the reference frame traveling with the laser,[12] which is ideal for accelerating and focusing. Some of these electrons will be trapped by the bubble if they have gained enough energy to catch up with the phase velocity of the bubble and be in proper phase when they fall back on axis at the rear of the wake. The trapped electrons can be accelerated by the strong electrostatic field inside the bubble to high energy with a quasi-monoenergetic energy spread under certain conditions. The maximum energy gain of the trapped electrons will be limited by the dephasing length ($L_d \propto {n_p}^{-3/2}$) and the average longitudinal electric field ($E_{max} \propto {n_p}^{1/2}$) within the wake. When the matching condition[13] (i.e., $a_0 \geq 2$ and $k_p w_0 \simeq 2\sqrt{a_0}$) is satisfied, it is given by

$$E_{max} \cong 1.7\left(\frac{P\,[\mathrm{TW}]}{100}\right)^{1/3}\left(\frac{10^{18}}{n_e\,[\mathrm{cm}^{-3}]}\right)^{2/3}\left(\frac{0.8}{\lambda_0(\mu\mathrm{m})}\right)^{4/3}, \quad (1)$$

where P is the laser power, λ_0 is the laser wavelength, and n_e is the plasma density. Both direct experimental optical diagnostics[14–17] and numerical simulations[18–20] show close correlations between the generation of collimated electron beams and the formation of the bubble. Although there are also some other injection schemes being explored, self-injection has advantages of reducing the technical complexity of experiment; thus, it is still the most common and simple experimental scheme.

Usually, it is difficult to improve the electron energy and the bunch charge simultaneously in the self-injected LWFA. The higher energy requires relatively low plasma density, while the bunch charge reduces with the decrease in the plasma density. For many applications, the large beam charge is a very important beam parameter, such as radiobiology,[21] radiotherapy,[22] femtosecond chemistry,[23] and industrial radiography.[24] For example, in the application of radiobiology, a low energy electron can be used for producing high absorption contrast bremsstrahlung radiation x-rays. And also, more energetic electron beams can be used for generating femtosecond intense x-rays or gamma rays through betatron radiation[25–27] or inverse Compton scattering.[28–32] In order to obtain more photons in above cases, more electrons are required. However, in LWFA, the number of electrons that can be loaded into a 3D nonlinear wake is limited by the beamloading effects,[33] which scales with the

a)Electronic addresses: lidz@iphy.ac.cn and lmchen@iphy.ac.cn

normalized volume of the bubble. According to Ref. 13, if $a_0 \geq 2$ and $k_p R \simeq k_p w_0 \simeq 2\sqrt{a_0}$, the maximum number of electrons can be given by

$$N_{max} \simeq \frac{1}{30}(k_p \mathrm{R})^3 \frac{1}{k_p r_e} \simeq 2.5 \times 10^9 \frac{\lambda_0[\mu\mathrm{m}]}{0.8} \sqrt{\frac{P[\mathrm{TW}]}{100}}, \quad (2)$$

where $a_0 = (eE)/(m\omega c)$ is the normalized laser strength parameter, w_0 is the laser spot size, R is the bubble radius, r_e is the electron classical radius, λ_0 is the laser wavelength, $k_p = 2\pi/\lambda_p$, where λ_p is the plasma wavelength.

As we know, the nonlinear evolution of a laser pulse propagating in the plasma is important for the initiation and termination of self-injection[19,34] and the properties of generated electron beams. When the laser pulse power $P \gg P_{cr}$ ($P_{cr} = 17(\mathrm{n_c}/\mathrm{n_e})\,\mathrm{GW}$ is the critical power for relativistic self-focusing[35]) and duration $\tau_L < 2\pi/\omega_{pe}$, the laser pulse would be self-guided in the plasma until depletion. During self-guiding, the continuous evolution of the laser pulse accompanied by the oscillation of a spot size, self-steepening, and self-compression may cause the deformation and elongation of the bubble, which will lead to a continuous and massive injection.[7,19,20,36–38]

In this paper, we report the experimental results of the generation of an electron bunch with a total charge of 620 pC (>100 MeV) at a plasma density of $6 \times 10^{18}\,\mathrm{cm}^{-3}$ by using 80 TW laser pulses to irradiate at a single-stage 3 mm Helium gas jet. By reducing the plasma density to $5 \times 10^{18}\,\mathrm{cm}^{-3}$, we obtained a quasi-monoenergetic electron bunch with the energy peaked at 249 MeV, the relative energy spread of 8%, and a total charge of 68 pC (>100 MeV). Two-dimensional (2D) particle-in-cell (PIC) simulations show that the unexpected large charge is due to the continuous injection caused by the self-steepening and self-compression of the laser pulse, which leads to the broadening and stretching of the bubble structure. Both the experiment and the simulation results indicate that a single-stage Helium plasma wakefield acceleration through this scheme is a feasible method to generate energetic and large charge electron beams.

II. EXPERIMENTAL SETUP

The experiment was performed with the 200TW laser system at the Key Laboratory for Laser Plasma in Shanghai Jiao Tong University. The laser system is operated with a central wavelength of 800 nm in the horizontal polarization. In the experiments, the system delivered 40 fs pulses at full width half-maximum with 80TW of power. As shown in Fig. 1, the pulses were focused by an f/20 off-axis-parabola onto a 3 mm supersonic gas jet. The measured vacuum focal spot shows a FWHM diameter of approximately 25 μm containing 28% of the total energy. The resultant focused peak laser intensity was up to $1.0 \times 10^{19}\,\mathrm{W/cm^2}$, corresponding to a normalized vector potential $a_0 \sim 2.2$. A top-view system was set to monitor the nonlinear Thomson side-scattering radiation at the second harmonic (400 nm) of the laser and image the plasma channel formation. A narrow bandpass filter with a transmission wavelength at 400 ± 20 nm was kept in front of the Charge-coupled Device (CCD) camera for collecting the second harmonic radiation. The generated electrons were dispersed by a 16 cm-long dipole magnet with a magnetic field strength of 0.98 T. An absolute calibrated image plate (IP) for electrons and x-rays (Fuji Film SR series)[39,40] covered with a 13 μm Al foil followed by a fixed fluorescent DRZ screen was used to simultaneously record the electron and the x-ray signal. The working gas during the experiments was pure helium, and the electron density was tuned by changing the backing pressure of gas jet. The gas jet can generate well-defined uniform gas density profiles in the range of $1 \times 10^{18}\,\mathrm{cm}^{-3} \sim 3 \times 10^{19}\,\mathrm{cm}^{-3}$, where the density information is based on hydrodynamic calculations as reported in Ref. 41.

III. EXPERIMENTAL RESULTS

In the experiment, we obtained an electron beam with the charge and energy higher than the normal scaling laws (Eq. (1–2)) of the typical bubble regime. The electron energy spectra obtained at different plasma densities are shown in Fig. 2. Fig. 2(a) is a typical electron spectrum at a plasma density $5 \times 10^{18}\,\mathrm{cm}^{-3}$; there is only one quasi-monoenergetic electron bunch with the energy peaked at 249 MeV (8% of relative energy spread) and a total charge of 68 pC. In the meanwhile, the corresponding emitted betatron x-ray photon number is estimated to be 3.8×10^6. When increasing the plasma density to $6 \times 10^{18}\,\mathrm{cm}^{-3}$, we obtained a continuous energy spectrum with the high energy tail extending over 0.6 GeV, and the total charge in this shot is measured up to 620 pC, as shown in Fig. 2(b). These features can be clearly seen in the lineout of the

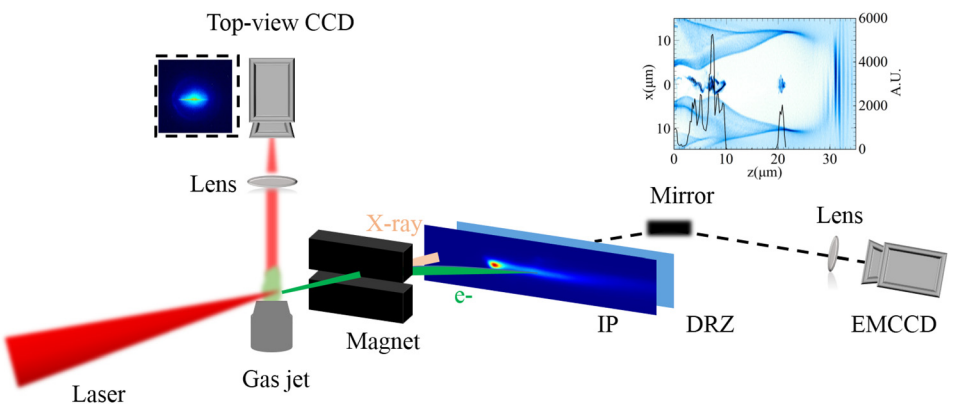

FIG. 1. Schematic of the experimental setup. All IPs are wrapped with a 13 μm Al foil. The inset beside the top-view CCD is a sample of the plasma channel. The inset IP before the DRZ shows a dispersed electron bunch. The inset above the mirror shows the duration of the electron bunches in the simulation.

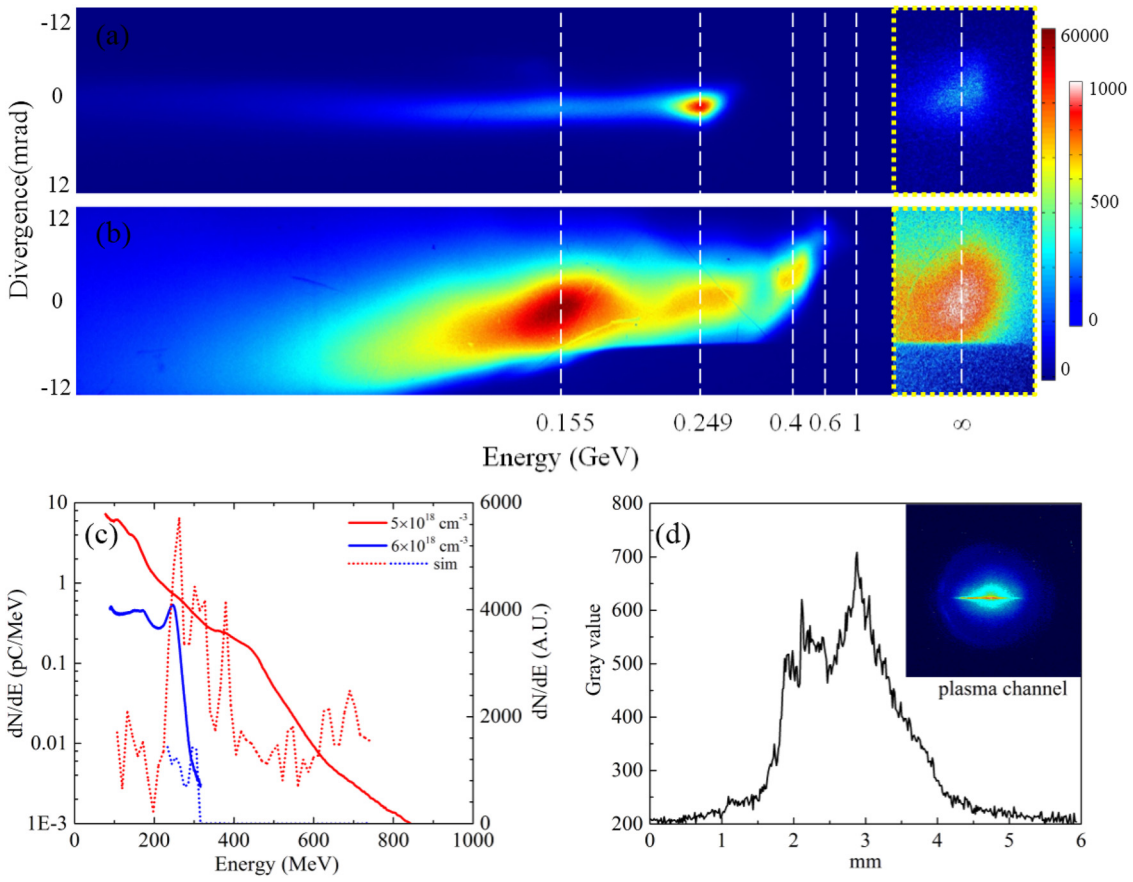

FIG. 2. Experimental results. (a) and (b) Images of electron spectra and corresponding betatron x-ray at the plasma density of $5 \times 10^{18}\,\mathrm{cm}^{-3}$ and $6 \times 10^{18}\,\mathrm{cm}^{-3}$, respectively. The larger color bar is for the electron bunch. (c) The corresponding angle integrated energy spectra of electrons for both plasma density and simulated energy spectra. (d) The lineout of the plasma channel and the inset is the corresponding Thomson scattering image of the plasma channel formed at density $6 \times 10^{18}\,\mathrm{cm}^{-3}$. The laser pulse propagated from right to left.

energy spectra shown in Fig. 2(c): the red line is the angle integrated energy spectra of electron energy at a plasma density of $6 \times 10^{18}\,\mathrm{cm}^{-3}$ and the blue line corresponds to the low density case. The dashed lines in Fig. 2(c) indicate simulated electron energy spectra. Moreover, the betatron radiation is greatly enhanced, the yield of x-ray (>7 keV) was much more than 3.1×10^{7}/shot, which is about 10-fold enhancement compared to the low density case.

Comparing these results with the normal scaling law for the maximum number of electrons loaded in a bucket shown in Eq. (2), we noticed that the measured charge of the electron bunch (620 pC) with energy beyond 100 MeV at the plasma density $6 \times 10^{18}\,\mathrm{cm}^{-3}$ is more than 1.5-fold of the expected value which is about 360 pC for a laser power of 80 TW employed in this experiment, and is almost 10-fold of the charge obtained at the plasma density of $5 \times 10^{18}\,\mathrm{cm}^{-3}$. Comparing the maximum electron energies achieved in these two particular shots, one can notice that higher electron energy was produced at the higher plasma density, which is contrary to the expected decreasing dephasing length. According to Eq. (1), the maximum energy gain of electrons is about 460 MeV for the high plasma density case, which is smaller than the electron bunch energy obtained from the experiment. Moreover, the maximum energy gain of experimental results at the plasma density of $6 \times 10^{18}\,\mathrm{cm}^{-3}$ is double than that at the low plasma density case. Though multi buckets acceleration in the longitudinal or transverse direction can explain the larger electron charge,[42–44] it cannot explain the boosted maximum energy. As shown in Fig. 3(a), we make plots of several measured data and previously published charge data of Refs. 7, 36, 44, and 45 as a function of the maximum accelerated energy in comparison with the scaling values of energy and charge. The solid red circles are our experimental results at the plasma density of $6 \times 10^{18}\,\mathrm{cm}^{-3}$, and the biggest circle is the same with the result presented in Fig. 2(a). The hollow red circle is the calculated value given by the scaling law of Ref. 13. The solid (hollow) black square, blue triangle, gray rhombus, and cyan pentagon are from Refs. 7, 36, 44, and 45 (calculated values), respectively. As we can see, both of these previous experimental results of Refs. 7 and 36 are smaller than the calculated values. Although the charge of the electron bunch is much higher in Ref. 44, which is due to the multiple-bubble wake structure caused by the multiple intensity peaks of the laser pulse, and most of electrons' energy is below 40 MeV, while our experimental results are either maximum energy or beam charge larger than the scaling laws. Instabilities of our data are most likely due to shot-to-shot changes in the plasma density and fluctuations in the laser beam parameters. In Ref. 45, there are also some data with the beam charge or maximum energy

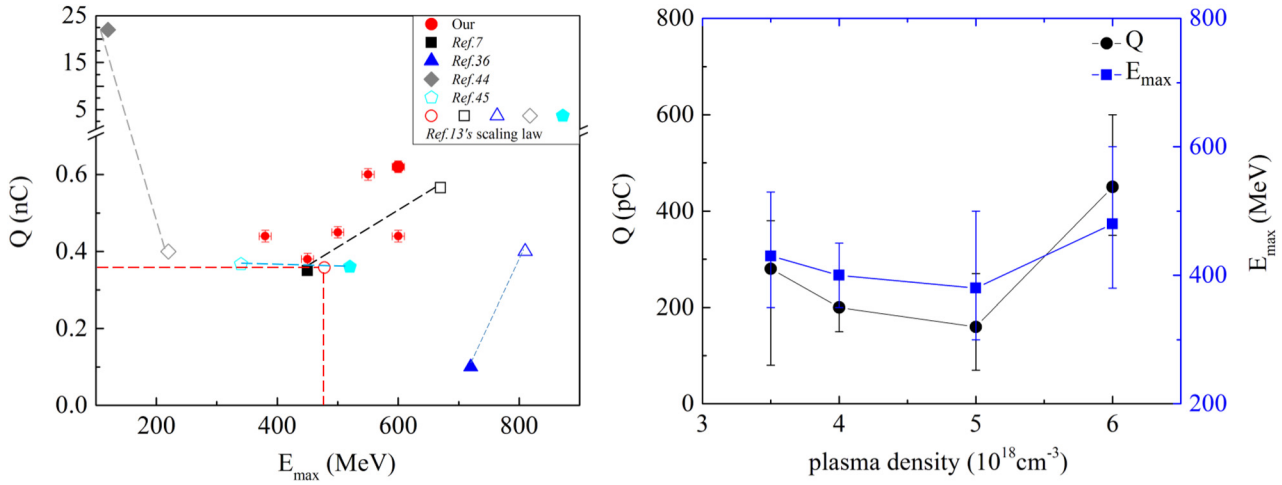

FIG. 3. Experimental results. (a) Beam charge, maximum energy of our results at the plasma density of $6 \times 10^{18}\,\mathrm{cm}^{-3}$ (solid red circles),[7] (solid black square),[36] (solid blue triangle),[44] (solid gray rhombus),[45] (solid cyan pentagon), and corresponding calculated values based on equations (1) and (2) (the corresponding hollow shapes). (b) The black circles and the blue triangles are the charge in electron beams and the maximum energy as a function of the plasma density.

larger than the scaling laws. It is lightly mentioned by multi buckets trapping or beam driven acceleration. The relationship between the beam charge and the maximum energy as a function of plasma density is shown in Fig. 3(b). As we can see, the average beam charge and maximum energy at the plasma density of $6 \times 10^{18}\,\mathrm{cm}^{-3}$ are larger than those at the low density case.

In order to understand the underlying physics, we monitored the plasma channel length. As shown in Fig. 2(d), there is only one plasma channel for the large charge shot, in which length is about 2.9 mm. It excludes the process that the electron charge increased nonlinearly due to the coherent superposition of laser spots.[43] At the plasma density $6 \times 10^{18}\,\mathrm{cm}^{-3}$, according to the scaling law,[13] the pump depletion length is $L_{pd} = c\,\tau_L(\omega_0/\omega_p)^2 \approx 3.3\,\mathrm{mm}$ and the dephasing length is $L_d = \left(\frac{2\sqrt{a_0}}{3\pi}\right)\left(\frac{\omega_0}{\omega_p}\right)^2 \lambda_p \approx 1.62\,\mathrm{mm}$, where c is the light speed in vacuum, τ_L is the laser pulse duration, λ_p is the plasma wavelength, and ω_0 and ω_p are the laser and plasma angular frequencies. The dephasing length L_d much shorter than the gas length and the boosted maximum electron energy indicate that the acceleration process is different from the normal bubble regime. The measured plasma channel length agrees approximately with the estimated L_{pd} value and nearly equals to the gas length ($\sim$3 mm). Thus, the acceleration mechanism may not be the mode transition from LWFA to plasma-wakefield accelerator (PWFA),[46] which is confirmed by our simulation to be discussed below.

IV. SIMULATION RESULTS

In order to understand the acceleration mechanism of generating a large charge electron beam in the experiment, 2D PIC simulations have been carried out using the KLAPS code.[47,48] P-polarized 800 nm laser pulses propagating in the z-direction with $a_0 = 3.0$ are focused onto a radius of 21 μm at the entrance of the fully ionized plasma. The pulse has a Gaussian transverse profile and a sin-square longitudinal shape with the pulse duration $\tau_{\mathrm{FWHM}} = 40$ fs. The plasma density is $6 \times 10^{18}\,\mathrm{cm}^{-3}$ with a linear up-ramp of 100 μm at the front, followed by a constant density over 2.8 mm, and then a linear down-ramp of 100 μm at the rear side. In the simulation, we used the box size of $80 \times 160\,\mu\mathrm{m}^2$ with 8 macro particles per cell with longitudinal and transverse resolutions of $\Delta z = 0.025\,\mu$m and $\Delta x = 0.2\,\mu$m, respectively. We will show that two distinct stages can be identified in our simulations.

Fig. 4 shows the multiple injection and acceleration processes accompanied by the laser pulse and bubble evolution. At the first stage, a bubble structure driven by the laser pulse expands and contracts with the oscillation of the laser spot size. The expansion of the bubble initiates self-injection of electrons from the sheath, then the stabilization and the contraction of bubble terminate the injection. As shown in Figs. 4(a) and 4(e), an electron bunch has been injected and accelerated with a small betatron oscillation amplitude. At this stage, the profile of the laser pulse electric field has not been modified much, as shown in Fig. 5(a). The maximum energy of the first injected electron bunch can be accelerated to over 400 MeV with the quasi-monoenergetic energy distribution, as shown in Figs. 4(c) and 4(g). The second stage begins at 5.6 ps, when the second injection process initiates due to the stretching of the bubble structure in the longitudinal direction, as shown in Figs. 4(b) and 4(f). Accompanied by the onset of the second injection, almost all electrons at the rear sheath of the elongated bubble can be trapped. The second continuously injected electron bunch with the relatively large charge can be accelerated to higher energy than the normal scaling limit. It is due to the elongation of the wakefield, as shown in Figs. 4(d) and 4(h), which leads to the increase in the dephasing length. In the simulation, the first injected electron bunch never reaches the front of the first bubble and the laser pulse sustains the wakefield for the whole interaction process. All these features exclude the acceleration mechanism from being the mode transition from LWFA to PWFA.

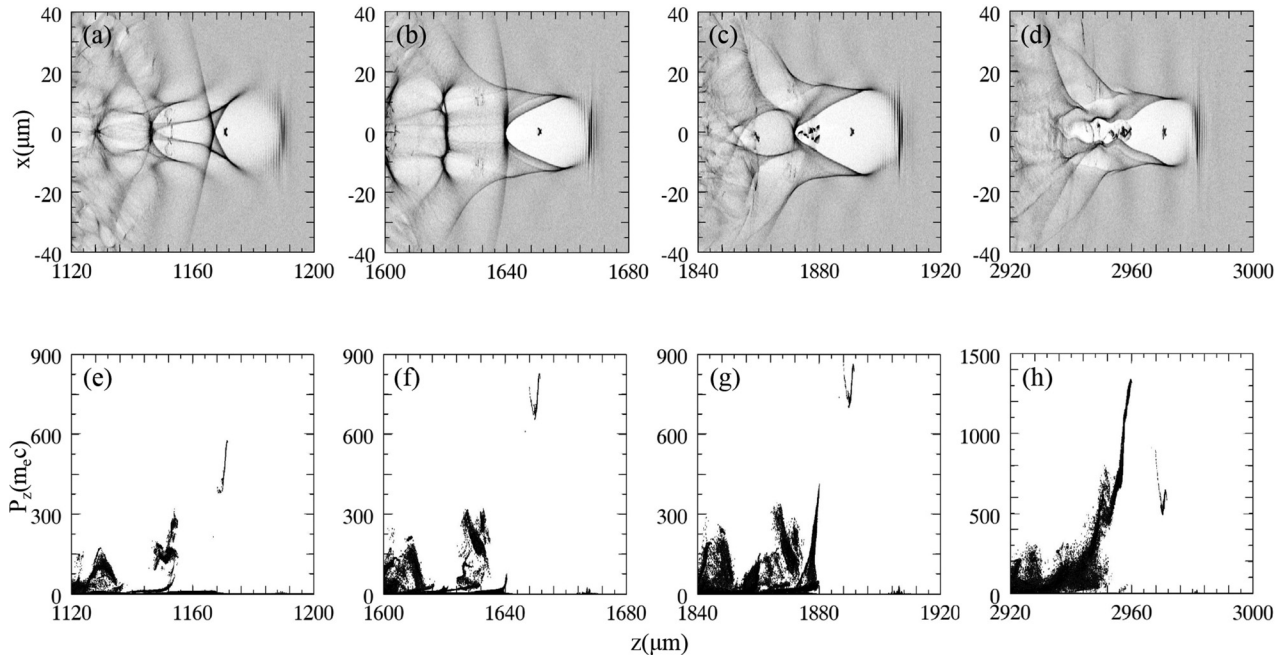

FIG. 4. 2D-PIC simulation results. (a)–(d) The electron density distribution, (e)–(h) the phase space (z-p_z) of electrons with $p_z > 6\ m_ec$. (a) and (e) Corresponding to t = 4 ps; (b) and (f) the onset of the second injection, corresponding to t = 5.6 ps; (c) and (g) the dephasing point of the first bunch, corresponding to t = 6.4 ps; and (d) and (h) the end of simulation, corresponding to t = 10 ps.

At the second stage, the laser pulse self-steepens and self-compresses as propagating in the plasma, leading to the broadening and stretching of the bubble, as shown in Figs. 4(b)–4(d) and 5(b)–5(d). During this process, the significant erosion of the laser pulse front forms a sharp front and an asymmetric laser field E_x, eventually resulting in a few-cycle laser pulse. Then, the carrier envelope phase effects may play a dominant role in stimulating transverse oscillations of the bubble.[38] As shown in Figs. 5(f)–5(h), all of these effects deform the bubble field structure and change the location of the wake potential minimum relative to the laser pulse, so a large amount of electrons can be trapped by the larger bucket during the process.

In order to clarify the acceleration mechanism, we analyzed the evolution of laser normalized strength parameter a_0 and two typical electron trajectories and energy of the first and the second injected electron bunches, as shown in Fig. 6. The red line in Fig. 6(a) reveals the evolution of a_0, which

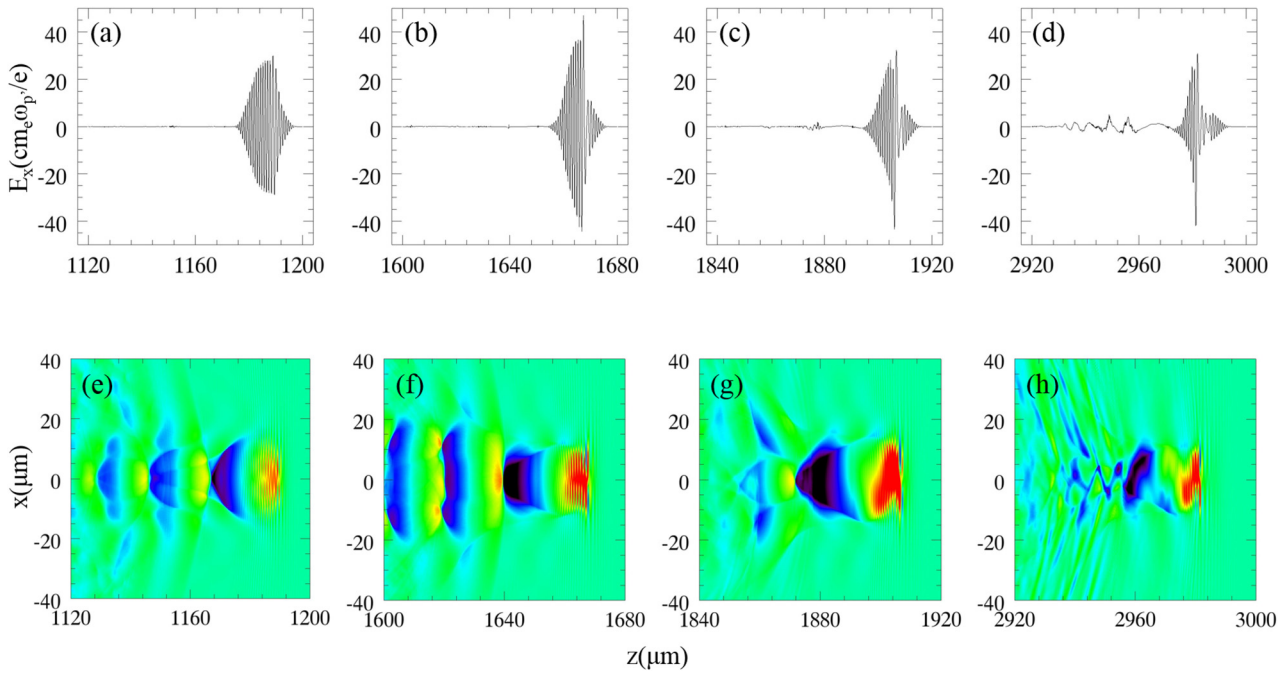

FIG. 5. The evolution of the laser pulse electric field and transverse distribution of the wakefield. (a)–(d) The laser's electric field at t = 4, 5.6, 6.4, and 10 ps, respectively; (e)–(h) the transverse distribution of the longitudinal wakefield at the corresponding time. And $\omega_{p'}$ is the normalized value used in the simulations, corresponding to $c/\omega_{p'} = 1\ \mu$m.

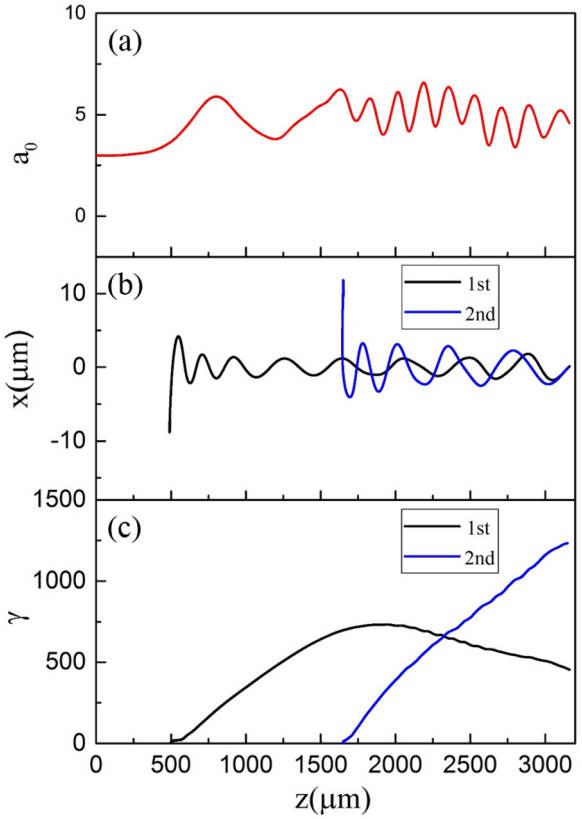

FIG. 6. The evolution of the normalized laser strength parameter a_0 and the typical behavior of two electron bunches. (a) The red line is the evolution of a_0; (b) the black (blue) line is a typical electron in the first (second) bunch, respectively. The average oscillation amplitudes for the first and the second electron bunches are 1.3 μm and 2.8 μm, respectively. (c) γ factor evolution of these two electrons as shown in (b), respectively.

oscillates slowly due to self-focusing and defocusing of the laser pulse propagating within the plasma at the first stage. Then, at the second stage, the oscillation of a_0 becomes quicker, while the laser spot size varies quickly. And we can see that the second electron bunch is injected during this process and triggered by a sharp increase in the laser intensity due to the significant self-focusing and self-steepening of the laser pulse, as shown by the blue line in Figs. 6(b) and 4(b)–4(d). Moreover, we can find that the oscillation amplitude of the second injected electron bunch is larger than the first one by comparing the electron trajectories in Fig. 6(b). It is because that the oscillation and asymmetric deformation of the bubble structure can be effectively coupled to the transverse momentum of the second injected electron bunch, leading to the betatron oscillation radiation enhancement.[20,37,38] The transverse evolution of the laser pulse and the electron trapping efficiency should be more intense and higher in the 3D simulation compared with the 2D simulation due to the multi-dimensional effects. Thus, the normalized laser strength parameter a_0 used in the simulations is a little larger than the experimental value. However, the phenomena described above, i.e., the elongation of bubble and the subsequent continuous electron injection with high charge and large oscillation amplitude, have already been discussed in Ref. 19, which is based on 3D simulations, supporting the physical process described in our 2D simulations. Therefore, we can make some semi-quantitative calculation and comparison between the simulation results and the experimental results. As shown in Fig. 6(c), the acceleration of the second electron bunch lasts till the end of the simulation with the maximum energy up to 630 MeV, which agrees well with the experimental results. The inset above the mirror in Figs. 1 and 4(d) shows that the second bunch duration in the simulation is about 30fs, thus the current intensity can be estimated as 20 kA. The simulated electron energy spectra at the plasma density of $5 \times 10^{18}\,\mathrm{cm}^{-3}$ and $6 \times 10^{18}\,\mathrm{cm}^{-3}$ are shown in Fig. 2(c). The normalized transverse emittance at energy slices of 130 ± 10 MeV, 260 ± 10 MeV, and 380 ± 10 MeV are 30π mm mrad, 18π mm mrad, and 31π mm mrad, respectively, for the plasma density of $6 \times 10^{18}\,\mathrm{cm}^{-3}$. And the normalized transverse emittance at energy slices of 300 ± 10 MeV is about 6π mm mrad for the plasma density of $5 \times 10^{18}\,\mathrm{cm}^{-3}$. The geometric emittance of the electron beams in the simulations is 0.01π mm mrad and 0.03π mm mrad for low and high plasma density case.

V. CONCLUSION

In conclusion, we have presented the experimental results of LWFA at different plasma densities with similar laser conditions. At the plasma density of $5 \times 10^{18}\,\mathrm{cm}^{-3}$, we obtained an electron bunch with the quasi-monoenergetic peak at 249 MeV, 68 pC charge. However, when we slightly increase the plasma density to $6 \times 10^{18}\,\mathrm{cm}^{-3}$, an electron bunch with a continuous spectrum extending up to 0.6 GeV and charge up to 620 pC was obtained, and the current intensity was estimated as 20 kA. In this case, the beam charge obtained from the experiment is almost 10-fold of the low density case. It is far more beyond the normal scaling law estimation. Moreover, the betatron radiation x-ray photon number at the high plasma density is much larger than the low density case. It suggests a totally different injection and acceleration process for the high density case. According to our simulation, the boosted energy and the electron charge are resulted from the stretching and deformation of the bubble structure, which is caused by the nonlinear evolution of the laser pulse. The high energy and large charge of electrons are beneficial for enhancing the yield and energy of x-ray/ γ-ray or positrons by inverse Compton scattering or irradiating on high Z materials target.

ACKNOWLEDGMENTS

We thank F. Liu and X. L. Ge for the help on operating the laser facility, and thank F. Li for participating in discussion. This work was supported by the National Basic Research Program of China (2013CBA01500), the National Key Scientific Instrument and Equipment Development Project (2012YQ120047), the National Natural Science Foundation of China (Nos. 11334013, 11421064, 11374210, and 11305185), the CAS key program (KGZD-EW-T05), and the MOST International Collaboration (2014DFG02330).

[1]T. Tajima and J. M. Dawson, Phys. Rev. Lett. **43**, 267 (1979).
[2]S. P. D. Mangles, C. D. Murphy, Z. Najmudin, A. G. R. Thomas, J. L. Collier, A. B. Dangor, E. J. Divall, P. S. Foster, J. G. Gallacher,

C. J. Hooker, D. A. Jaroszyanski, A. J. Langley, W. B. Mori, P. A. Norreys, F. S. Tsung, R. Viskop, B. R. Walton, and K. Krushelnick, Nature **431**, 535 (2004).
[3]J. Faure, Y. Glinec, A. Pukhov, S. Kiselev, S. Gordienko, E. Lefebvre, J. P. Rousseau, F. Burgy, and V. Malka, Nature **431**, 541 (2004).
[4]C. G. R. Geddes, Cs. Toth, J. van Tilborg, E. Esarey, C. B. Schroeder, D. L. Bruhwiler, C. Nieter, J. R. Cary, and W. P. Leemans, Nature **431**, 538 (2004).
[5]W. P. Leemans, B. Nagler, A. J. Gonsalves, Cs. Tóth, K. Nakamura, C. G. R. Geddes, E. Esarey, C. B. Schroeder, and S. M. Hooker, Nat. Phys. **2**, 696 (2006).
[6]N. A. M. Hafz, T. M. Jeong, I. W. Choi, S. K. Lee, K. H. Pae, V. V. Kulagin, J. H. Sung, T. J. Yu, K.-H. Hong, and T. Hosokai, Nat. Photonics **2**, 571 (2008).
[7]S. Kneip, S. R. Nagel, S. F. Martins, S. P. D. Mangles, C. Bellei, O. Chekhlov, R. J. Clarke, N. Delerue, E. J. Divall, G. Doucas, K. Ertel, F. Fiuza, R. Fonseca, P. Foster, S. J. Hawkes, C. J. Hooker, K. Krushelnick, W. B. Mori, C. A. J. Palmer, K. Ta Phuoc, P. P. Rajeev, J. Schreiber, M. J. V. Streeter, D. Urner, J. Vieira, L. O. Silva, and Z. Najmudin, Phys. Rev. Lett. **103**, 035002 (2009).
[8]C. E. Clayton, J. E. Ralph, F. Albert, R. A. Fonseca, S. H. Glenzer, C. Joshi, W. Lu, K. A. Marsh, S. F. Martins, W. B. Mori, A. Pak, F. S. Tsung, B. B. Pollock, J. S. Ross, L. O. Silva, and D. H. Froula, Phys. Rev. Lett. **105**, 105003 (2010).
[9]X. M. Wang, R. Zgadzaj, N. Fazel, Z. Y. Li, S. A. Yi, X. Zhang, W. Henderson, Y.-Y. Chang, R. Korzekwa, H.-E. Tsai, C.-H. Pai, H. Quevedo, G. Dyer, E. Gaul, M. Martinez, A. C. Bernstein, T. Borger, M. Spinks, M. Donovan, V. Khudik, G. Shvets, T. Ditmire, and M. C. Downer, Nat. Commun. **4**, 1988 (2013).
[10]H. T. Kim, K. H. Pae, H. J. Cha, I. J. Kim, T. J. Yu, J. H. Sung, S. K. Lee, T. M. Jeong, and J. Lee, Phys. Rev. Lett. **111**, 165002 (2013).
[11]W. P. Leemans, A. J. Gonsalves, H.-S. Mao, K. Nakamura, C. Benedetti, C. B. Schroeder, Cs. Tóth, J. Daniels, D. E. Mittelberger, S. S. Bulanov, J.-L. Vay, C. G. R. Geddes, and E. Esarey, Phys. Rev. Lett. **113**, 245002 (2014).
[12]I. Kostyukov, A. Pukhov, and S. Kiselev, Phys. Plasmas **11**, 5256 (2004).
[13]W. Lu, M. Tzoufras, C. Joshi, F. S. Tsung, W. B. Mori, J. M. Vieira, R. A. Fonseca, and L. O. Silva, Phys. Rev. Spec. Top. –Accel. Beams **10**, 061301 (2007).
[14]P. Dong, S. A. Reed, S. A. Yi, S. Kalmykov, G. Shvets, M. C. Downer, N. H. Matlis, W. P. Leemans, C. McGuffey, S. S. Bulanov, V. Chvykov, G.Kalintchenko, K. Krushelnick, A. Maksimchuk, T. Matsuoka, A. G. R. Thomas, and V. Yanovsky, Phys. Rev. Lett. **104**, 134801 (2010).
[15]M. H. Helle, D. Kaganovich, D. F. Gordon, and A. Ting, Phys. Rev. Lett. **105**, 105001 (2010).
[16]A. Buck, M. Nicolai, K. Schmid, C. M. S. Sears, A. Savert, J. M. Mikhailova, F. Krausz, M. C. Kaluza, and L. Veisz, Nature Phys. **7**, 543 (2011).
[17]A. Sävert, S. P. D. Mangles, M. Schnell, E. Siminos, J. M. Cole, M. Leier, M. Reuter, M. B. Schwab, M. Möller, K. Poder, O. Jäckel, G. G. Paulus, C. Spielmann, S. Skupin, Z. Najmudin, and M. C. Kaluza, Phys. Rev. Lett. **115**, 055002 (2015).
[18]F. S. Tsung, W. Lu, M. Tzoufras, W. B. Mori, C. Joshi, J. M. Vieira, L. O. Silva, and R. A. Fonseca, Phys. Plasmas **13**, 056708 (2006).
[19]S. Y. Kalmykov, A. Beck, S. A. Yi, V. N. Khudik, M. C. Downer, E. Lefebvre, B. A. Shadwick, and D. P. Umstadter, Phys. Plasmas **18**, 056704 (2011).
[20]Y. Ma, L. Chen, D. Li, W. Yan, K. Huang, M. Chen, Z. Sheng, K. Nakajima, T. Tajima, and J. Zhang, Sci. Rep. **6**, 30491 (2016).
[21]O. Rigaud, N. O. Fortunel, P. Vaigot, E. Cadio, M. T.Martin, O. Lundh, J. Faure, C. Rechatin, V. Malka, and Y. A. Gauduel, Cell Death Dis. **1**, e73 (2010).
[22]O. Lundh, C. Rechatin, J. Faure, A. Ben-Ismail, J. Lim, C. De Wagter, W. De Neve, and V. Malka, Med. Phys. **39**, 3501 (2012).
[23]V. Malka, J. Faure, and Y. A. Gauduel, Mutat. Res., Rev. Mutat. Res. **704**, 142 (2010).
[24]A. Ben-Ismaïl, O. Lundh, C. Rechatin, J. K. Lim, J. Faure, S. Corde, and V. Malka, Appl. Phys. Lett. **98**, 264101 (2011).
[25]S. Kneip, C. McGuffey, J. L. Martins, S. F. Martins, C. Bellei, V. Chvykov, F. Dollar, R. Fonseca, C. Huntington, G. Kalintchenko, A. Maksimchuk, S. P. D. Mangles, T. Matsuoka, S. R. Nagel, C. A. J. Palmer, J. Schreiber, K. Ta Phuoc, A. G. R. Thomas, V. Yanovsky, L. O. Silva, K. Krushelnick, and Z. Najmudin, Nat. Phys. **6**, 980 (2010).
[26]S. Cipiccia, M. R. Islam, B. Ersfeld, R. P. Shanks, E. Brunetti, G. Vieux, X. Yang, R. C. Issac, S. M. Wiggins, G. H. Welsh, M. P. Anania, D. Maneuski, R. Montgomery, G. Smith, M. Hoek, D. J. Hamilton, N. R. C. Lemos, D. Symes, P. P. Rajeev, V. O. Shea, J. M. Dias, and D. A. Jaroszynski, Nat. Phys. **7**, 867 (2011).
[27]K. Huang, Y. F. Li, D. Z. Li, L. M. Chen, M. Z. Tao, Y. Ma, J. R. Zhao, M. H. Li, M. Chen, M. Mirzaie, N. Hafz, T. Sokollik, Z. M. Sheng, and J. Zhang, Sci. Rep. **6**, 27633 (2016).
[28]K. Ta Phuoc, S. Corde, C. Thaury, V. Malka, A. Tafzi, J. P. Goddet, R. C. Shah, S. Sebban, and A. Rousse, Nat. Photonics **6**, 308–311 (2012).
[29]S. Chen, N. D. Powers, I. Ghebregziabher, C. M. Maharjan, C. Liu, G. Golovin, S. Banerjee, J. Zhang, N. Cunningham, A. Moorti, S. Clarke, S. Pozzi, and D. P. Umstadter, Phys. Rev. Lett. **110**, 155003 (2013).
[30]N. D. Powers, I. Ghebregziabher, G. Golovin, C. Liu, S. Chen, S. Banerjee, J. Zhang, and D. P. Umstadter, Nat. Photonics **8**, 28 (2013).
[31]G. Sarri, D. J. Corvan, W. Schumaker, J. M. Cole, A. Di Piazza, H. Ahmed, C. Harvey, C. H. Keitel, K. Krushelnick, S. P. D. Mangles, Z. Najmudin, D. Symes, A. G. R. Thomas, M. Yeung, Z. Zhao, and M. Zepf, Phys. Rev. Lett. **113**, 224801 (2014).
[32]K. Khrennikov, J. Wenz, A. Buck, J. Xu, M. Heigoldt, L. Veisz, and S. Karsch, Phys. Rev. Lett. **114**, 195003 (2015).
[33]M. Tzoufras, W. Lu, F. S. Tsung, C. Huang, W. B. Mori, T. Katsouleas, J. Vieira, R. A. Fonseca, and L. O. Silva, Phys. Rev. Lett. **101**, 145002 (2008).
[34]H. Xu, W. Yu, P. Lu, V. K. Senecha, F. He, B. Shen, L. Qian, R. Li, and Z. Xu, Phys. Plasmas **12**, 013105 (2005).
[35]E. Esarey, C. B. Schroeder, and W. P. Leemans, Rev. Mod. Phys. **81**, 1229–1285 (2009).
[36]D. H. Froula, C. E. Clayton, T. Doppner, K. A. Marsh, C. P. J. Barty, L. Divol, R. A. Fonseca, S. H. Glenzer, C. Joshi, W. Lu, S. F. Martins, P. Michel, W. B. Mori, J. P. Palastro, B. B. Pollock, A. Pak, J. E. Ralph, J. S. Ross, C. W. Siders, L. O. Silva, and T. Wang, Phys. Rev. Lett. **103**, 215006 (2009).
[37]E. N. Nerush and I. Yu Kostyukov, Phys. Rev. Lett. **103**, 035001 (2009).
[38]W. C. Yan, L. M. Chen, D. Z. Li, L. Zhang, N. Hafz, J. Dunn, Y. Ma, K. Huang, L. N. Su, M. Chen, Z. M. Sheng, and J. Zhang, Proc. Natl. Acad. Sci. U. S. A. **111**, 5825 (2014).
[39]K. A. Tanaka, T. Yabuuchi, T. Sato, R. Kodama, Y. Kitagawa, T. Takahashi, T. Ikeda, Y. Honda, and S. Okuda, Rev. Sci. Instrum. **76**, 013507 (2005).
[40]J. Y. Mao, L. M. Chen, L. T. Hudson, J. F. Seely, L. Zhang, Y. Q. Sun, X. X. Lin, and J. Zhang, Rev. Sci. Instrum. **83**, 043104 (2012).
[41]T. Hosokai, K. Kinoshita, T. Watanabe, K. Yoshii, T. Ueda, A. Zhidokov, M. Uesaka, K. Nakajima, M. Kando, and H. Kotaki, in *Proceedings of the European Particle Accelerator Conference* (2002), pp. 981–983.
[42]E. Guillaume, A. Döpp, C. Thaury, A. Lifschitz, J-P. Goddet, A. Tafzi, F. Sylla, G. Iaquanello, T. Lefrou, P. Rousseau, K. Ta Phuoc, and V. Malka, Phys. Rev. Accel. Beams **18**, 061301 (2015).
[43]Y. Ma, L. M. Chen, M. H. Li, Y. F. Li, J. G. Wang, M. Z. Tao, Y. J. Han, J. R. Zhao, K. Huang, W. C. Yan, D. Z. Li, Z. Y. Chen, J. L. Ma, Y. T. Li, Z. M. Sheng, and J. Zhang, Phys. Plasmas **22**, 083102 (2015).
[44]B. Shen, Y. Wu, K. Dong, B. Zhu, Y. Gu, L. Ji, C. Jiao, J. Teng, W. Hong, Z. Zhao, L. Cao, X. Wang, and M. Y. Yu, Phys. Plasmas **19**, 033106 (2012).
[45]C. McGuffey, T. Matsuoka, S. Kneip, W. Schumaker, F. Dollar, C. Zulick, V. Chvykov, G. Kalintchenko, V. Yanovsky, A. Maksimchuk, A. G. R. Thomas, K. Krushelnick, and Z. Najmudin, Phys. Plasmas **19**, 063113 (2012).
[46]P. E. Masson-Laborde, M. Z. Mo, A. Ali, S. Fourmaux, P. Lassonde, J. C. Kieffer, W. Rozmus, D. Teychenné, and R. Fedosejevs, Phys. Plasmas **21**, 123113 (2014).
[47]M. Chen, Z. M. Sheng, J. Zhen, Y. Y. Ma, and Zhang, J. Comput. Phys. **25**, 43 (2008).
[48]W.-M. Wang, P. Gibbon, Z.-M. Sheng, and Y.-T. Li, Phys. Rev. E. **91**, 013101 (2015).